# Structural and Magnetic Effects of Successive Protonations of Oxo Bridges in High-Valent Manganese Dimers

**Michael J. Baldwin,† Timothy L. Stemmler,† Pamela J. Riggs-Gelasco,† Martin L. Kirk,‡ James E. Penner-Hahn,† and Vincent L. Pecoraro*,†**

*Contribution from the Departments of Chemistry, The University of Michigan, Ann Arbor, Michigan 48109-1055, and The University of New Mexico, Albuquerque, New Mexico 87131-1096*

*Received June 20, 1994*®

**Abstract:** The preparation and characterization of $[Mn^{IV}(salpn)(\mu\text{-}OH)]_2(CF_3SO_3)_2$, $\mathbf{1H_2}(CF_3SO_3)_2$, the first bis-(hydroxo)-bridged manganese(IV) dimer, is reported. Along with the previously reported complexes $[Mn^{IV}(salpn)(\mu\text{-}O)]_2$, **1**, and $[Mn^{IV}(salpn)]_2(\mu\text{-}O)(\mu\text{-}OH)(CF_3SO_3)$, $\mathbf{1H}(CF_3SO_3)$, this provides the first series of oxo-bridged manganese complexes which are isolated in three different protonation states of the bridges without a change in the other ligands or the manganese oxidation state. The effects of oxo bridge protonations on the structure and magnetism of these Mn(IV) dimers are studied using this series of complexes. Each successive protonation of the oxo bridges results in a 2200 $cm^{-1}$ decrease in the energy of the lowest energy (presumably, phenolate-to-manganese) charge transfer transition, a lengthening of the Mn–Mn distance, and a dramatic decrease in the antiferromagnetic coupling, without a significant change in the manganese X-ray absorption edge energies. The edge energies are all within 0.3 eV of each other, at ca. 6553 eV. The extended X-ray absorption fine structure spectra indicate that the Mn–Mn distance increases from 2.73 Å for **1** to 2.83 and 2.93 Å with successive protonations. Temperature-dependent magnetic susceptibility measurements show that the antiferromagnetic coupling of **1** decreases from $J = -92$ $cm^{-1}$ to $J = -48$ $cm^{-1}$ upon the first protonation, and to $J = -6$ $cm^{-1}$ upon the second protonation. Such a low coupling as found for $\mathbf{1H_2}(CF_3SO_3)_2$ is unprecedented for Mn(IV) dimers. Understanding the effects of protonation on the electronic and geometric structure of high-valent $Mn^{IV}_2(\mu\text{-}O)_2$ units is important, as this core has been proposed to exist in the oxygen-evolving complex (OEC) of photosystem II. The possible effects of protonation state changes on S-state advancement and the proposed different configurations of $S_1$ and $S_2$ are discussed.

## Introduction

The oxygen in the atmosphere is produced as a byproduct of the water oxidation which supplies reducing equivalents and protons for photosynthesis in green plants and photosynthetic bacteria. This water oxidation occurs at a redox-active tetranuclear manganese site of undetermined structure in photosystem II, known as the oxygen-evolving complex (OEC). The OEC sequentially provides reducing equivalents to $P680^+$ (through the redox-active tyrosine, $Y_z$) following photoexcitation of P680. After the OEC is oxidized four times, the manganese site is reduced as a result of the four-electron oxidation of water to molecular oxygen and four protons.[1] The ability of the OEC to undergo four one-electron oxidations followed by a four-electron reduction, coupled to water oxidation, is remarkable but poorly understood.

The different oxidation states involved in the reaction cycle of the OEC are referred to as the S-states, $S_0$ through $S_4$ being the relevant states for the normal reactivity of the OEC, with the subscript referring to the number of stored oxidation equivalents. $S_1$ is the resting state of the dark-adapted site and is believed to be in the $Mn^{III}_2Mn^{IV}_2$ oxidation state.[2,3] Three flashes of light advance the OEC from $S_0$ through $S_3$, and a fourth flash brings the OEC to the transient $S_4$ which spontaneously oxidizes water by four electrons to return to $S_0$. Changes in the X-ray absorption edge energy suggest that each oxidation from $S_0$ through $S_2$ results in an increase in manganese oxidation state. The question of whether manganese oxidation occurs with the higher S-state transitions has generated some controversy, and there is disagreement as to whether there is a significant shift in the X-ray absorption edge upon advancement from $S_2$ to $S_3$.[3,4]

Extended X-ray absorption fine structure (EXAFS) studies have shown that at least the $S_1$- and $S_2$-states of the OEC contain more than one Mn–Mn vector of 2.7Å and one or more Mn–Mn vectors of 3.3 Å.[3,5] The 2.7 Å distances almost certainly correspond to high-valent $Mn_2(\mu\text{-}O)_2$ units, which have been shown to have similar Mn–Mn distances.[6–10] The possible configurations of the manganese ions in the tetranuclear site are constrained but not defined by the EXAFS data. The manganese connectivity has also been probed by studies of the changes in magnetic susceptibility in different S-states. An interesting result of the magnetic studies is the *increase* in magnetic moment upon advancing from $S_1$ to $S_2$, which might

* To whom correspondence should be addressed.
† The University of Michigan.
‡ The University of New Mexico.
® Abstract published in *Advance ACS Abstracts,* November 1, 1994.

(1) Babcock, G. T.; Barry, B. A.; Debus, R. J.; Hoganson, C. W.; Atamian, M.; McIntosh, L.; Sithole, I.; Yocum, C. F. *Biochemistry* **1989**, *28*, 9557–9565.
(2) Riggs, P. J.; Mei, R.; Yocum, C. F.; Penner-Hahn, J. E. *J. Am. Chem. Soc.* **1992**, *114*, 10650–10651.
(3) Klein, M. P.; Sauer, K.; Yachandra, V. K. *Photosynth. Res.* **1993**, *38*, 265–277.
(4) Ono, T.; Noguchi, T.; Inoue, Y.; Kusunoki, M.; Matsushita, T.; Oyanagi, H. *Science* **1992**, *258*, 1335–1337.
(5) Penner-Hahn, J. E.; Fronko, R. M.; Pecoraro, V. L.; Yocum, C. F.; Betts, S. D.; Bowlby, N. R. *J. Am. Chem. Soc.* **1990**, *112*, 2549–2557.
(6) Larson, E.; Lah, M. S.; Li, X.; Bonadies, J. A.; Pecoraro, V. L. *Inorg. Chem.* **1992**, *31*, 373–378.
(7) Wieghardt, K. *Angew. Chem., Int. Ed. Engl.* **1989**, *28*, 1153–1172.
(8) Stebler, M.; Ludi, A.; Bürgi, H.-B. *Inorg. Chem.* **1986**, *25*, 4743–4750.
(9) Goodson, P. A.; Glerup, J.; Hodgson, D. J.; Michelsen, K.; Pedersen, E. *Inorg. Chem.* **1990**, *29*, 503–508.
(10) Hagan, K. S.; Armstrong, W. H.; Hope, H. *Inorg. Chem.* **1988**, *27*, 967–969.

0002-7863/94/1516-11349$04.50/0 

be expected to correspond to a loss of one unpaired electron and a resulting decrease in magnetic moment.[11]

These structural and magnetic studies are complicated somewhat by the apparent existence of two different configurations of the manganese site in both $S_1$ and $S_2$. The $S_1$-state has different properties depending on whether it is in the "active" or dark-adapted "resting" state,[12] with the active state appearing to be paramagnetic while the resting state has been shown to be diamagnetic.[13] Two configurations of the $S_2$-state are characterized by different electron paramagnetic resonance (EPR) signals, either a multiline signal at $g = 2$ or a signal at $g = 4.1$, which can be preferentially isolated by illumination of $S_1$-centers at selected temperatures.[14] Although the overall reaction at the OEC requires the generation of four protons, the proton stoichiometry of each S-state is likely to be important in the reaction cycle,[15] and may be involved in the variations observed for the different $S_1$- and $S_2$-configurations.

In order to understand the possible roles that protonation of the high-valent $Mn_2(\mu\text{-}O)_2$ units may play in the catalytic cycle of the OEC, we have studied the effects of protonation on the chemistry, structure, and magnetic properties of the Mn(IV) dimer $[Mn(salpn)(\mu\text{-}O)]_2$, **1**. The X-ray crystal structure of this complex shows the Mn−Mn distance to be 2.73 Å,[6,16] similar to that seen for the $S_1$- and $S_2$-states of the OEC. Gohdes and Armstrong showed that the Mn(IV) ions are strongly antiferromagnetically coupled,[16] as had been reported for other high-valent $Mn_2(\mu\text{-}O)_2$ complexes. This complex is an efficient catalyst for hydrogen peroxide disproportionation,[17,18] apparently mimicking the alternative substrate ($H_2O_2$) catalase activity that cycles between the $S_0$- and $S_2$-states of the OEC.[19] The catalase activity of $[Mn(salpn)(\mu\text{-}O)]_2$ was shown to be inhibited by a single protonation of the complex, which was believed to occur on one of the oxo bridges.[20] EXAFS data showed that the Mn−Mn distance increased by 0.1 Å upon protonation, and electrochemical data indicated that the reduction potential increased substantially upon protonation.[20] By preparing the series of complexes $[Mn(X\text{-}salpn)(\mu\text{-}O)]_2$, where X-salpn are derivatives of salpn with electron-donating or -withdrawing groups on the phenolate rings and X = 5-$OCH_3$ (**2**), 5-Cl (**3**), 3,5-di-Cl (**4**), or 5-$NO_2$ (**5**), we have been able to probe the relationship between manganese reduction potentials and protonations.[21] Over a range of potentials (over 600 mV) and p$K_a$'s (over 7 units), a linear correlation exists between the reduction potentials of the $[Mn(X\text{-}salpn)(\mu\text{-}O)]_2$ complexes and the p$K_a$'s of the $[Mn(X\text{-}salpn)(\mu\text{-}O, \mu\text{-}OH)]_2^+$ complexes, indicating that the protonation chemistry and redox chemistry of these strongly coupled units are intimately related.

In continuing our studies on the protonation chemistry of $[Mn(salpn)(\mu\text{-}O)]_2$, we show definitively that the protonation occurs on the oxo bridge, and we report the preparation and characterization of the doubly protonated complex. This provides the first series of $Mn_2O_2$ complexes protonated on neither, one, and both oxo bridges without a change in oxidation state of the manganese. This has allowed us to examine the effects of successive protonations of the oxo bridges on the structural and magnetic properties of these complexes without the complications of changes in oxidation state or ligands.

## Experimental Section

**Preparation of Complexes.** Chemicals were obtained from Aldrich and solvents were Burdick and Jackson brand obtained from Baxter Scientific, with no further purification, unless otherwise specified. Low temperatures (−50 °C) for sample preparations were provided by dry ice−acetonitrile baths, and low-temperature reactions were done under dry nitrogen to prevent water condensation in the solutions. Moisture sensitive samples were vacuum filtered and dried under dry nitrogen.

The ligands X-salpn$H_2$ were prepared by the Schiff base condensation of 1 equiv of 1,3-diaminopropane and 2 equiv of the appropriately substituted salicylaldehyde (i.e., X-2-hydroxybenzaldehyde) in methanol.

**$[Mn^{IV}(salpn)(\mu\text{-}O)]_2$, 1, $Mn^{IV}$(5-Cl-salpn)$(\mu\text{-}O)]_2$, 3, and $Mn^{IV}$-(3,5-di-Cl-salpn)$(\mu\text{-}O)]_2$, 4.** For **1**, 0.43 g (1 mmol) of $Mn^{III}$(salpn)(acac), prepared as described previously,[17] was dissolved in 50 mL of acetonitrile. Approximately 0.5 mL of 50% hydrogen peroxide was added to the stirring solution, dropwise. The solution changed immediately from dark green to red-brown with precipitation of a red-brown microcrystalline solid. The solid was suction filtered (>90% yield). The solid was then recrystallized from DMF at 100 °C upon standing at room temperature. **1**·2DMF: Anal. Calcd for $Mn_2C_{40}H_{46}N_6O_8$: Mn, 12.9; C, 56.61; H, 5.46; N, 9.90. Found: Mn, 12.9; C, 56.65; H, 5.35; N, 9.97. **3**·2DMF: Anal. Calcd for $Mn_2C_{40}H_{42}N_6O_8Cl_4$: Mn, 11.1; C, 48.70; H, 4.29; N, 8.52. Found: Mn, 10.5; C, 48.85; H, 4.23; N, 8.49. **4**·2DMF: Anal. Calcd for $Mn_2C_{40}H_{38}N_6O_8Cl_8$: Mn, 9.8; C, 42.73; H, 3.41; N, 7.47. Found: Mn, 9.3; C, 42.71; H, 3.66; N, 7.69.

**$[Mn^{IV}$(5-$OCH_3$-salpn)$(\mu\text{-}O)]_2$, 2.** For **2**, 0.25 g of $Mn^{III}$(5-$OCH_3$-salpn)(acac) was dissolved in 50 mL of DMF and stirred in the air for 10 days. The resulting brown solid was filtered, washed with DMF and ether, and pumped dry by vacuum (yield 20% after 10 days, with additional solid collected after more time). Anal. Calcd for $Mn_2C_{38}H_{40}N_4O_{10}$: Mn, 13.4; C, 55.48; H, 4.90; N, 6.81. Found: Mn, 13.1; C, 55.37; H, 4.87; N, 7.00.

**$[Mn^{IV}$(5-$NO_2$-salpn)$(\mu\text{-}O)]_2$, 5.** For **5**, 3.7 g of 5-$NO_2$-salpn$H_2$ and 0.8 g of NaOH were dissolved in 200 mL of hot methanol, and 3.6 g of $Mn(ClO_4)_2{\cdot}6H_2O$, dissolved in 20 mL of methanol, was added. After stirring for 1 h at room temperature, the $Mn^{II}$(5-$NO_2$-salpn) product was filtered as an orange precipitate. This was dissolved in 100 mL of DMA and stirred overnight. The solid (yield after several days >80% from initial reactants) was filtered and recrystallized by redissolving in DMA and adding several volumes of DMF. The microcrystalline solid was filtered and washed with DMF. **5**·3DMF: Anal. Calcd for $Mn_2C_{43}H_{49}N_{11}O_{17}$: Mn, 10.0; C, 46.88; H, 4.48; N, 13.98. Found: Mn, 9.9; C, 46.83; H, 4.27; N, 13.67.

**$[Mn^{IV}_2$(salpn)$_2(\mu\text{-}O)(\mu\text{-}OH)]^+$, 1H($CF_3SO_3$).** For 1H($CF_3SO_3$), 0.7 g of **1** (1 mmol) was slurried in 200 mL of chloroform at room temperature, and 0.25 g of pyridinium triflate (1.1 mmol), dissolved in 2 mL of acetonitrile, was added. The mixture was stirred for 30 min and filtered. The solid was brought up in 100 mL of chloroform, stirred briefly, filtered, rinsed with chloroform until no color was observed in the filtrate, washed with ether, air dried, and pumped on under vacuum for 30 min (65% yield). Anal. Calcd for $Mn_2C_{35}H_{33}N_4O_9F_3S$: Mn, 12.9; C, 49.31; H, 3.90; N, 6.57. Found: Mn, 12.8; C, 49.14; H, 4.02; N, 6.52.

**$[Mn^{IV}_2$(5-$NO_2$-salpn)$_2(\mu\text{-}O)(\mu\text{-}OH)]^+$, 5H($CF_3SO_3$).** For 5H($CF_3SO_3$), 0.17 g of **5** was slurried in 75 mL of acetonitrile, 2 mL of 0.1 M triflic acid in acetonitrile was added, and the mixture was stirred for 2 min. The mixture was gravity filtered into a flask containing 200 mL of ether with stirring. This mixture was then suction filtered, and the purple solid was washed with ether, briefly air dried, and pumped on under vacuum for 2 h (50% yield). Anal. Calcd for

(11) Sivaraja, M.; Philo, J. S.; Lary, J.; Dismukes, G. C. *J. Am. Chem. Soc.* **1989**, *111*, 3221−3225.
(12) Beck, W. F.; de Paula, J. C.; Brudvig, G. W. *Biochemistry* **1985**, *24*, 3035−3043.
(13) Koulougliotis, D.; Hirsh, D. H.; Brudvig, G. W. *J. Am. Chem. Soc.* **1992**, *114*, 8322−8323.
(14) Haddy, A.; Dunham, W. R.; Sands, R. H.; Aasa, R. *Biochim. Biophys. Acta* **1992**, *1099*, 25−34.
(15) Lavergne, J.; Junge, W. *Photosynth. Res.* **1993**, *38*, 279−296.
(16) Gohdes, J. W.; Armstrong, W. H. *Inorg. Chem.* **1992**, *31*, 368−373.
(17) Larson, E. J.; Pecoraro, V. L. *J. Am. Chem. Soc.* **1991**, *113*, 3810−3818.
(18) Larson, E. J.; Pecoraro, V. L. *J. Am. Chem. Soc.* **1991**, *113*, 7809−7810.
(19) Frasch, W. D.; Mei, R. *Biochim. Biophys. Acta* **1987**, *891*, 8−14.
(20) Larson, E. J.; Riggs, P. J.; Penner-Hahn, J. E.; Pecoraro, V. L. *J. Chem. Soc., Chem. Commun.* **1992**, 102−103.
(21) Baldwin, M. J.; Gelasco, A.; Pecoraro, V. L. *Photosynth. Res.* **1993**, *38*, 303−308.

$Mn_2C_{35}H_{29}N_8O_{17}F_3S$: Mn, 10.6; C, 40.71; H, 2.83; N, 10.85. Found: Mn, 10.2; C, 40.70; H, 3.11; N, 11.34.

**$[Mn^{IV}(salpn)(\mu\text{-}OH)]_2^{2+}$, $1H_2(CF_3SO_3)_2$.** For $1H_2(CF_3SO_3)_2$, 0.17 g of **1**·2DMF was slurried in 25 mL of $CH_2Cl_2$ and cooled to −50 °C under $N_2$, and 4 mL of 0.1 M triflic acid in acetonitrile was added 1 mL at a time over about 10 min. The mixture was stirred at −50 °C for 1 h and then left to stand overnight at −70 °C. The cold solution was then suction filtered through a glass frit under nitrogen flow, washed 2× each with $CH_2Cl_2$ and ether, dried under the nitrogen stream for 2 h, and pumped on under vacuum for 1 h (40% yield). Anal. Calcd for $Mn_2C_{36}H_{34}N_4O_{12}F_6S_2$: Mn, 11.0; C, 43.13; H, 3.42; N, 5.59. Found: Mn, 10.8; C, 42.66; H, 3.33; N, 5.52.

**$[Mn^{IV}(5\text{-}NO_2\text{-}salpn)(\mu\text{-}OH)]_2^{2+}$, $5H_2(CF_3SO_3)_2$.** For $5H_2(CF_3SO_3)$, 0.18 g of **5** was slurried in 25 mL of $CH_2Cl_2$ at −50 °C, and 4 mL of 0.1 M triflic acid in acetonitrile was added 1 mL at a time over about 10 min. No obvious color change occurred after 30 min, so the mixture was warmed to room temperature. Within 30 min, a green solid had precipitated. This solid was suction filtered under a $N_2$ stream, dried under the nitrogen stream, and pumped on under vacuum for 30 min (yield 90%). Anal. Calcd for $Mn_2C_{36}H_{30}N_8O_{20}F_6S_2$: Mn, 9.3; C, 36.56; H, 2.56; N, 9.48. Found: Mn, 9.1; C, 36.7; H, 2.71; N, 9.53.

**UV−Vis Absorption Spectroscopy.** UV−vis absorption spectra were obtained using a Perkin-Elmer Lamda 9 UV−Vis−IR spectrophotometer. Low-temperature spectra were obtained by use of a custom-made quartz dewar with suprasil quartz windows. Cryogenic baths consisting of dry ice slurries in acetonitrile (−50 °C), carbon tetrachloride (−20 °C), or acetone (−78 °C) were used to cool the samples in the dewar.

**X-ray Absorption Spectroscopy. A. X-ray Absorption Measurements.** Manganese K-edge EXAFS spectra were measured at both the Stanford Synchrotron Radiation Laboratory (SSRL), beamline VII-3, and the National Synchrotron Light Source (NSLS), beamlines X10-C and X19-A. Both facilities were operating under dedicated conditions (3.0 GeV/100 mA and 2.5 GeV/200 mA, respectively). At X10-C, a Si(111) single-crystal monochromator was used, while at X19-A and VII-3, Si(220) double-crystal monochromators were used. At all three locations, monochromators were detuned by 50% for harmonic rejection. The beam size at VII-3 and X10-C was 2 mm × 10 mm, while at X19-A the beam size was 2 mm × 15 mm. All monochromators were calibrated using a $KMnO_4$ powder internal standard, with the pre-edge peak assigned at 6543.3 eV. Spectra were measured in transmission mode using ionization chambers filled with nitrogen gas. At VII-3 and X10-C, samples were held at 10 K using an Oxford Instruments He flow cryostat, while at X19-A, samples were held at 77 K using a Janis liquid nitrogen finger dewer. Transmission samples were prepared in a glovebox by grinding the sample with boron nitride. Samples were placed in 1 mm thick Al cells with 40 $\mu$m Kapton windows. All spectra were recorded from 6300 to 7400 eV with scan times of approximately 35 min and a $k$ spacing of 0.05 Å$^{-1}$. Two or three spectra were collected and averaged for each sample.

**B. Data Analysis.** X-ray absorption spectroscopy (XAS) spectra were averaged independently for each data set collected at each location. A pre-edge subtraction was performed by fitting the pre-edge region with a smooth polynomial which was extrapolated into the EXAFS region and subtracted. A series of polynomials were then fit to the EXAFS region and subtracted, and the edge data were normalized. The data were converted to $k$ space using $E_0 = 6555$ eV and weighted by $k^3$ in order to compensate for the diminishing amplitude at high $k$. The EXAFS signal $k^3\chi(k)$ vs $k$ was truncated at 1.0 and 11.5 Å$^{-1}$ and then Fourier transformed. Data were Fourier-filtered to isolate each peak in the Fourier transform. Initial fits were performed on Fourier-filtered data; however, all the best-fit bond lengths, coordination numbers, and Debye−Waller factors in Table 2 were determined by fitting unfiltered data with a $k$ window of 1.0−11.5 Å$^{-1}$ (consistent with previous fits of protein data[5]). A "goodness of fit" parameter, $F$, was calculated as $F = \{[k^6(\text{data} - \text{fit})^2]/(\text{no. of points})\}^{1/2}$ for each fit. Fits of the data with larger $k$ ranges up to 13 Å$^{-1}$ produced a better apparent $F$ value, but with no change in calculated bond lengths and without an increase in resolution of the first two shells of scatterers relative to the fit with a smaller $k$ window. Theoretical models for the EXAFS amplitude and phase functions were calculated using the program FEFF 3.25.[22] Scale factor and threshold energies were calibrated by fitting the appropriate shells of EXAFS data from Mn(IV) models which have been crystallographically characterized with theoretical models generated for identical coordination environments. Theoretical models were calculated for Mn−O, Mn−N, and Mn−Mn interactions and a scale factor of 0.9, and $\Delta E_0$ values of 6.0, 6.0, and 14.6 were used to fit the respective interactions in the EXAFS data. Least-squares fits were used to determine Mn−ligand distances and coordination numbers according to established methods.[23]

**Magnetic Susceptibility.** Magnetic susceptibility measurements were made on well-ground solid samples in the temperature range 2.2−300 K and in an applied magnetic field of 5 kG using a Quantum Design Model MPMS superconducting quantum interference device (SQUID) magnetometer. The magnetometer was calibrated using a recrystallized $HgCo(NCS)_4$ standard[18] and a palladium cylinder. Pascal's constants were used to determine the diamagnetism of the complexes. The samples (25−60 mg) were packed in a clear gelatin capsule with the top half inverted to prevent movement of the powdered samples. The capsule was housed in a clear soda straw which was fixed to the magnetometer drive rod. The measured diamagnetism of the sample holder assembly was approximately 25% of the measured magnetization at 300 K of the samples with the lowest magnetic moments. The data analysis was performed as described in the text on a Macintosh computer using the program Kaleidagraph (Abelbeck Software) with its standard library routine for function minimization.

## Results

**Protonation of Oxo Bridges.** We have previously shown that the complex **1** could be protonated by a weak acid such as pyridinium ion,[20] and that the strength of the acid required for the protonation depended on the substituent X for the series of complexes $[Mn^{IV}(X\text{-}salpn)(\mu\text{-}O)]_2$, **1**−**5**.[21] It had been assumed that this protonation occurred on one of the bridging oxo ions. In order to definitively assign this protonation position, the complex **1** was prepared with $^{18}O$ in the bridging positions. Upon protonation with pyridinium perchlorate to $1H(ClO_4)$, the sharp O−H stretching peak in the IR spectrum shifted from 3539 cm$^{-1}$ in the sample with $^{16}O$ bridges to 3529 cm$^{-1}$ in the sample with $^{18}O$ bridges. This is very close to the shift of 11.6 cm$^{-1}$ calculated for an isolated O−H stretch at that frequency. This indicates definitively that the protonation occurs on a bridging oxo, since those are the only positions which would produce an isotope shift in the O−H stretch under these conditions.

Addition of further equivalents of an acid with a p$K_a$ close to that of the singly protonated complex does not result in any further rapid reaction (although solutions of the protonated complexes decompose to a Mn(III) product over time). Addition of another equivalent of a substantially stronger acid in acetonitrile does result in a rapid reaction. Stronger acids of noncoordinating anions, such as triflic acid, cause a bleaching of the solution at room temperature to a light yellow-brown, while reaction with HCl result in formation of the monomeric $Mn^{IV}(salpn)Cl_2$.[24] If the temperature is reduced to −50 °C, addition of 2 equiv of triflic acid results in a deep blue-green solution $[1H_2(CF_3SO_3)_2]$. The successive additions of the first and second equivalents of triflic acid result in the shifts of the lowest energy charge transfer band (presumably a phenolate-to-manganese CT) to higher wavelength (490 to 550 to 630 nm) as shown in Figure 1, producing a color change from red-brown to purple to blue-green.

(22) Rehr, J. J.; Albers, R. C.; Mustre de Leon, J. *Physica* **1989**, *B158*, 417.

(23) Teo, B. K. In *EXAFS Spectroscopy, Techniques and Application*; Teo, B. K., Joy, D. C., Eds.; Plenum: New York, 1981; pp 13−58.

(24) Machonkin, T. E.; Larson, E. J.; Pecoraro, V. L. *J. Chem. Soc., Chem. Commun.*, submitted for publication.

**Table 1.** Reduction Potentials for **1**−**5** and Acid Dissociation Constants for $\mathbf{1H^+}$−$\mathbf{5H^+}$ and $\mathbf{1H_2^{2+}}$−$\mathbf{5H_2^{2+}}$, in Order of Increasing Electron-Withdrawing Capacity of X

| | X = 5-$OCH_3$ (**2**) | X = H (**1**) | X = 5-Cl (**3**) | X = 3,5-$Cl_2$ (**4**) | X = 5-$NO_2$ (**5**) |
|---|---|---|---|---|---|
| $E_{1/2}$ (mV vs SCE) of **1**−**5**[a] | −588 | −507 | −335 | −235 | +20 |
| p$K_a$ in $CH_3CN$[b] of $\mathbf{1H^+}$−$\mathbf{5H^+}$ [a] | 14.1 ± 0.4 | 13.4 ± 0.2 | 11.5 ± 0.4 | 10.8 ± 0.3 | 6.8 ± 0.3 |
| p$K_a$ in $CH_3CN$[b] of $\mathbf{1H_2^{2+}}$−$\mathbf{5H_2^{2+}}$ | 10−12 | 8−11 | 7−9 | 5−8 | <4 |

[a] Reported previously by Baldwin et al.[21] [b] Norton suggests a −7.5 ± 1 p$K_a$ unit correction to convert $CH_3CN$ p$K_a$'s to aqueous p$K_a$'s.[34]

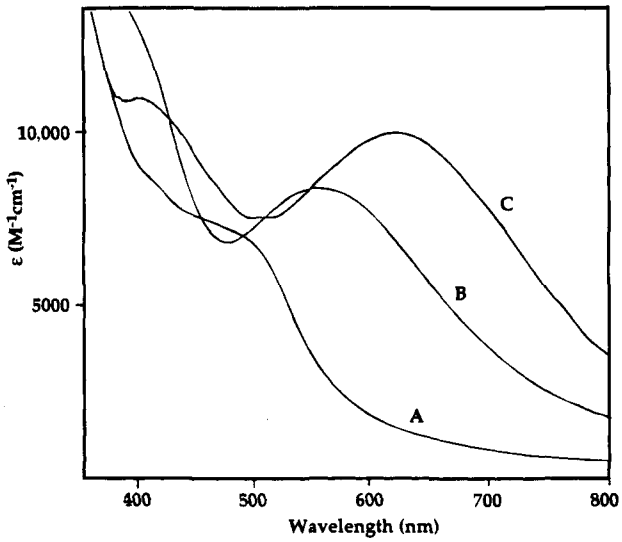


**Figure 1.** UV−vis absorption spectra in $CH_2Cl_2$ of (A) **1** at room temperature, (B) $\mathbf{1H}(CF_3SO_3)$ at room temperature, and (C) $\mathbf{1H_2}(CF_3SO_3)_2$ at −50 °C.

Warming the blue-green solution of $\mathbf{1H_2}(CF_3SO_3)_2$ to room temperature results in rapid bleaching of the solution to a light yellow-brown. Additions of 1 and 2 equiv of base to the cold blue-green solution results in color changes to purple and red-brown, respectively, indicating complete reversibility of the protonation reactions. The doubly protonated $\mathbf{1H_2}(CF_3SO_3)_2$ can be obtained as a solid from methylene chloride, and the solid is stable at room temperature provided it is kept very dry. Addition of the blue-green solid to acetonitrile at room temperature results in decomposition to the yellow-brown solution, while addition to acetonitrile at −50 °C results in a blue-green solution with the same absorption spectrum as that obtained from $\mathbf{1H_2}(CF_3SO_3)_2$ prepared *in situ*.

Approximate p$K_a$ values for the complexes $[Mn(X\text{-salpn})(OH)]_2^{2+}$ were estimated by addition of 2 equiv of acids of varying p$K_a$ values in acetonitrile to **1**−**5**. The p$K_a$ range below which rapid reaction beyond the singly protonated state occurs was observed and assumed to be near the p$K_a$ value for $\mathbf{1H_2^{2+}}$−$\mathbf{5H_2^{2+}}$. Although this does not provide a precise value for the p$K_a$, and is complicated by the irreversible reaction of the doubly protonated complexes at room temperature, it provides a p$K_a$ range for comparison to the p$K_a$ values we have reported for the complexes $\mathbf{1H^+}$−$\mathbf{5H^+}$.[21] These values are reported in Table 1. The values obtained indicate that the p$K_a$ for the second proton to be added to **1**−**5** is around 3−5 p$K_a$ units lower than that of the first proton. This is nearly the same as the 4−5 unit difference between the first and second p$K_a$'s of several $[Cr^{III}(\mu\text{-OH})]_2^{4+}$ complexes.[25] The p$K_a$ of each complex decreases as more electron-withdrawing substituents are placed on the X-salpn ligand. This is reflected in the effects of different solvents on the various protonated derivatives of **1**−**5**. While addition of the solid $\mathbf{1H_2}(CF_3SO_3)_2$ to acetonitrile results in decomposition at room temperature [*vide supra*], addition to methanol results in a purple solution, indicating that deprotonation of one of the oxo bridges occurs more rapidly than decomposition. The complex **5** cannot be doubly protonated in acetonitrile, but $\mathbf{5H_2}(CF_3SO_3)_2$ can be prepared by addition of $HCF_3SO_3$ to a slurry of **5** in methylene chloride. Due to the extreme insolubility of $\mathbf{5H_2}(CF_3SO_3)_2$ in methylene chloride, this can be accomplished at room temperature without decomposition. At −50 °C, the second protonation does not appear to occur. Addition of solid $\mathbf{5H_2}(CF_3SO_3)_2$ to acetonitrile at room temperature results in the purple $\mathbf{5H}(CF_3SO_3)$, and addition to methanol results in precipitation of the red-brown **5**. In general, the ease in obtaining pure solid samples of these complexes is more dependent upon their solubility properties and solvent interactions than on their inherent stability. The solution stability of the singly protonated complexes is also solvent dependent. Although it is water sensitive, $\mathbf{1H^+}$ is substantially more stable in methanol than in acetonitrile. This most likely indicates that the decomposition mechanism for solutions of $\mathbf{1H^+}$ is the equilibrium with a small amount of $\mathbf{1H_2^{2+}}$ (around 0.01%, based on the p$K_a$ differences), which rapidly and irreversibly decomposes to the Mn(III) product. The irreversibility of this latter reaction drives the equilibrium toward this decomposition product.

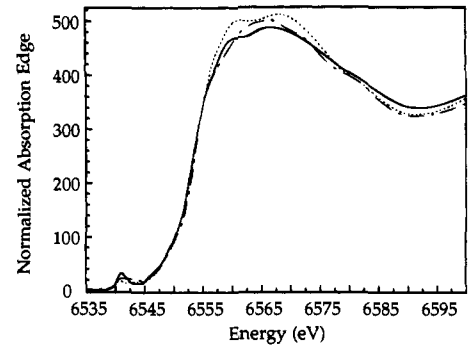


**Figure 2.** Normalized Mn K X-ray absorption edges for $[Mn(salpn)(\mu\text{-O})]_2$, **1** [6553.5 eV; dotted-dashed line]; $[Mn_2(salpn)_2(\mu\text{-O})(\mu\text{-OH})](CF_3SO_3)$, $\mathbf{1H}(CF_3SO_3)$ [6553.2 eV; solid line], and $[Mn(salpn)(\mu\text{-OH})]_2(CF_3SO_3)_2$, $\mathbf{1H_2}(CF_3SO_3)_2$ [6553.3 eV; short dashed line].

**X-ray Absorption Spectra.** Figure 2 shows a comparison of the normalized X-ray absorption near edge structure (XANES) spectra for **1**, $\mathbf{1H}(CF_3SO_3)$, and $\mathbf{1H_2}(CF_3SO_3)_2$. Normalized spectra for all three complexes show the same edge energy and similar edge features. The first inflection point for each edge occurs at ca. 6553 eV, which is consistent with the edge energies of other Mn(IV) models that we have studied,[26] and varies by only 0.3 eV through the series. These Mn(IV) edge energies are significantly higher than the edge energy measured for $Mn^{III}(salpn)(CH_3OH)_2(CF_3SO_3)$ [6550.9 eV]. The pre-edge peaks at about 6541 eV are due to 1s → 3d transitions. A pure 1s → 3d transition is forbidden by dipole selection rules. However, for noncentrosymmetric metal environments, the 1s → 3d transition gains intensity as a result of 3d + 4p mixing in the electronic ground state. The observed 1s → 3d intensity increases upon going from **1** to $\mathbf{1H}(CF_3SO_3)$, indicating

(25) Gafford, B. G.; Holwerda, R. A. *Inorg. Chem.* **1989**, *28*, 60−66.

(26) Riggs-Gelasco, P. A.; Penner-Hahn, J. E. Manuscript in preparation.

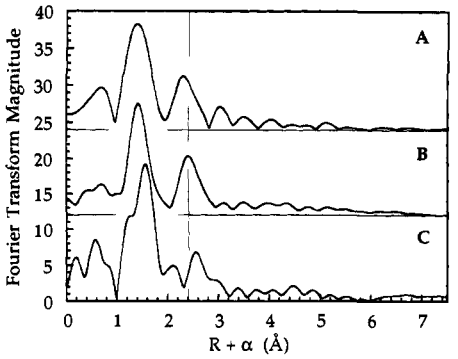


**Figure 3.** Fourier transforms of the EXAFS data obtained for (A) **1**, (B) **1**H($CF_3SO_3$), and (C) **1**$H_2(CF_3SO_3)_2$. Lines drawn at $R + \alpha = 2.4$ Å ($\alpha = -0.4$ Å) on each spectrum indicate the systematic shift in the second shell feature upon protonation of the oxo bridges. Data for (B) and (C) have been offset vertically by 12 and 24 units for clarity.

**Table 2.** Fitting Results for the Best Fit of All Data Sets with Mn−O and Mn−Mn Interactions in **1**, **1**$H^+$ and **1**$H_2^{2+}$ Using Theoretical Models

| | | Mn−N/O interaction | | | Mn−Mn interaction | | |
|---|---|---|---|---|---|---|---|
| complex | date[a] | $R$ (Å) | CN[b] | $\sigma^2$ [c] | $R$ (Å) | CN[b] | $\sigma^2$ [c] |
| **1** | I | 1.89 | 4.0 | 4.2 | 2.72 | 1.0 | 2.5 |
| | II | 1.90 | 4.0 | 3.4 | 2.73 | 1.0 | 2.8 |
| **1**H($CF_3SO_3$) | I | 1.90 | 5.0 | 4.3 | 2.83 | 1.0 | 0.6 |
| | II | 1.90 | 4.0 | 3.2 | 2.82 | 1.0 | 2.2 |
| **1**$H_2(CF_3SO_3)_2$ | II | 1.92 | 4.0 | 2.6 | 2.92 | 1.0 | 6.0 |
| | III | 1.92 | 4.0 | 1.3 | 2.94 | 1.0 | 4.7 |

[a] Data collected on the following dates and beamlines: I, 2/91, NSLS beamline X10-C (fits to these data, which were calibrated to preliminary X-ray data for **1**, were reported previously[20]); II, 8/93, NSLS beamline X19-A; III, 3/94, SSRL beamline 7-3. [b] Coordination numbers are given as the best fit integer value. [c] Debye−Waller factors are given in units of Å$^2 \times 10^3$.

increased Mn 4p character in the ground state of the monoprotonated species. Protonation of the second bridge to produce **1**$H_2(CF_3SO_3)_2$ causes a decrease in the intensity to slightly lower than that for **1**. The decrease in 1s → 3d intensity from **1** to **1**$H_2(CF_3SO_3)_2$ is consistent with the change expected on going from oxo to the less distorted hydroxo bridges.

EXAFS data for all three samples were Fourier-filtered over a $k$ range of 1.0−11.5 Å$^{-1}$, and the resulting Fourier transforms are shown in Figure 3. The Fourier transforms for **1** and **1**H($CF_3SO_3$) both show well-defined second shell Mn−Mn interactions consistent with $Mn_2(\mu\text{-}O)_2$ and $Mn_2(\mu\text{-}O)(\mu\text{-}OH)$ cores, respectively.[20] The outer shell structure for **1**$H_2(CF_3SO_3)_2$ is more complicated. However, there is one principal feature with approximately the same amplitude as that found for the Mn−Mn shell of **1**. The second shell peaks of **1**H($CF_3SO_3$) and **1**$H_2(CF_3SO_3)_2$ are shifted by 0.1 and 0.2 Å, respectively, relative to the feature seen in **1**. The Mn−Mn distance must therefore increase by ca. 0.1 Å with each protonation of the $Mn_2(\mu\text{-}O)_2$ core.

**A. First Shell Fitting Analysis.** Fits for the Mn−nearest neighbor ligand interactions were analyzed using both the unfiltered and Fourier-filtered EXAFS data over a variety of $k$ ranges. The average first shell bond lengths for **1**H($CF_3SO_3$) and **1**$H_2(CF_3SO_3)_2$ appear to increase slightly upon protonation of the oxo bridges. This is consistent with an approximately 0.1 Å increase in one-sixth of the bond lengths. Table 2 lists the average first shell bond lengths and coordination numbers calculated for all data sets. The apparent EXAFS bond length for **1** is ~0.02 Å shorter than the $1/k^3$ weighted average of the crystallographic bond lengths. This underestimate is most likely a reflection of the fact that shorter bond lengths tend to have smaller Debye−Waller factors and thus tend to make a larger contribution to the overall EXAFS.

For each sample, a single O or N wave could be used to fit the first shell EXAFS. However, the quality of the fit was relatively poor, and the best fit coordination number was unrealistically low. Attempts to fit the Mn−nearest neighbor interactions in the EXAFS of **1**, **1**H($CF_3SO_3$), and **1**$H_2(CF_3SO_3)_2$ with a short Mn−O and a longer Mn−N shell resulted in the refinement of one of the shells to the bond length found in the single shell analysis, while the remaining shell refined with an unrealistically high Debye−Waller factor. We attribute the poor fit quality and the low apparent coordination number to the fact that, on the basis of the crystallographic data,[6,16] the first shell in **1** and presumably in **1**H($CF_3SO_3$) and **1**$H_2(CF_3SO_3)_2$ consists of a mixture of Mn−O/N bonds with a wide range of bond lengths. There are three distinct types of Mn−nearest neighbors in **1**, at 1.81 Å (two Mn−oxo bonds), 1.92 Å (two Mn−O(phenolate) bonds), and 2.07 Å (two Mn−N bonds). These distances are too close to be separated by the resolution of the present data (resolution $\approx \pi/2k_{max} = 0.14$ Å) but are too far apart to be well modeled by the simple Gaussian distribution that is assumed when using a Debye−Waller damping term. This is in contrast to the EXAFS data for binuclear iron systems containing an oxo bridge which typically show two readily resolvable shells of Fe−O/N distances with a short (approximately 1.80 Å) Fe−O distance and longer (approximately 2.1 Å) Fe−N distances.[27] Zang and co-workers have also recently reported that Fe−oxo and Fe−hydroxo distances (1.82 and 1.99 Å, respectively) can be resolved in an $Fe_2(\mu\text{-}O)(\mu\text{-}OH)$ complex in which all other ligands are at about 2.2 Å.[28] We attribute the difference in behavior of our $Mn_2O_2$ complexes to the fact that they include Mn−phenolate bonds at an intermediate distance, precluding resolution of the different first shell distances.

**B. Second Shell Fitting Analysis.** In all three samples, both the Fourier-filtered and the unfiltered EXAFS data required a Mn−Mn interaction for a good fit. Fits using a 3.0 Å Mn−C component in place of the Mn−Mn component were substantially worse and, moreover, gave chemically unrealistic Debye−Waller factors. Interpretation of the Mn−Mn component is potentially complicated by the presence of Mn−C scattering from the salpn ligand (five carbons per Mn atom at bond lengths between 2.9 and 3.0 Å[6,16]). This could be particularly important for **1**$H_2(CF_3SO_3)_2$ since the Mn−C and Mn−Mn distances are very similar. However, when the data for **1**$H_2(CF_3SO_3)_2$ were fit with a Mn−Mn interaction and a Mn−C interaction, there was no change in the apparent Mn−Mn bond length (2.92 Å) and the Mn−C shell was highly disordered ($\sigma^2 = 40 \times 10^{-3}$ Å$^2$) at an average Mn−C distance of 3.4 Å. Attempts to fit the second shell of **1** and **1**H($CF_3SO_3$) with Mn−Mn and Mn−C interactions similarly gave a disordered Mn−C shell in addition to the well-defined Mn−Mn interaction. In no case did the fit improve significantly on including a Mn−C shell in addition to the Mn−Mn shell. Thus, it appears that, in all three cases, the Mn−C shell does not make a significant contribution to the observed EXAFS. This most likely is due to the fact that the Mn−C distances show the same disorder seen for the Mn−N/O first shell distances.

**Magnetic Studies.** Variable temperature magnetic susceptibility data were collected for **1**, **1**H($CF_3SO_3$), and **1**$H_2(CF_3SO_3)_2$, as well as for several of the phenolate-substituted derivatives, from 5 to 300 K (2.2−300 K for **1**$H_2(CF_3SO_3)_2$).

(27) Scarrow, R. C.; Maroney, M. J.; Palmer, S. M.; Que, L., Jr.; Roe, A. L.; Salowe, S. P.; Stubbe, J. *J. Am. Chem. Soc.* **1987**, *109*, 7857−7864.
(28) Zang, Y.; Pan, G.; Que, L., Jr.; Fox, B. G.; Münck, E. *J. Am. Chem. Soc.* **1994**, *116*, 3653−3654.

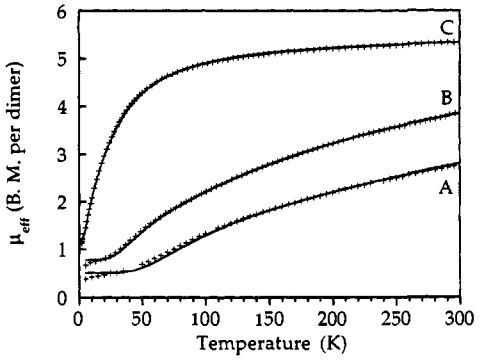


**Figure 4.** Temperature dependence of $\mu_{eff}$ for (A) **1**, (B) **1**H($CF_3SO_3$), and (C) **1**$H_2(CF_3SO_3)_2$. Data are represented by plus signs. The solid line is the best fit with **g** = 2.00 and $J$ and the percentage of $S = 2$ impurity allowed to vary, as described in the text.

**Table 3.** Exchange Coupling ($J$, $cm^{-1}$)[a] in the Various Protonation States of **1** and **5**

| derivative of X-salpn | $[MnLO]_2$ | $[Mn_2L_2(O,OH)]^+$ | $[MnL(OH)]_2^{2+}$ |
|---|---|---|---|
| X = H, **1** | −92 | −48 | −6 |
| X = 5-$NO_2$, **5** | −90 | −40 | −8[b] |

[a] Best fits for $J$ with **g** set at 2.00 and a term for an $S = 2$ impurity (<2.3% in all cases). [b] **g** = 1.79. The fit with **g** = 2.00 was poor; the best fit $J = -13$ $cm^{-1}$.

The data for the various protonation states of **1** are shown in Figure 4 as plus signs, with the solid lines representing the fits described below. The various derivatives for which magnetic susceptibility data were obtained are listed in Table 3. It can be seen from the data in Figure 4 that successive protonations of the oxo bridges cause a substantial increase in the room temperature magnetic moment compared to the strongly coupled $Mn_2(\mu\text{-}O)_2$ unit.

The spin Hamiltonian in eq 1 was employed in the analysis of the magnetic data for these Mn(IV)$_2$ ($S_1 = 3/2$, $S_2 = 3/2$) complexes to quantitate the magnetic coupling between the manganese ions. $S_1 = S_2 = 3/2$ are the spins of the two Mn-

$$H = -2J(S_1S_2) + \mathbf{g}\beta H(S_1 + S_2) \quad (1)$$

(IV) ions, and $J$ is the exchange interaction within the Heisenberg−Dirac−Van Vleck formalism. The $\mu_{eff}$ vs temperature data were fit to eq 2, with $\chi_M$ defined in eq 3, which is derived

$$\mu_{eff} = 2.828(\chi_M T)^{1/2} \quad (2)$$

$$\chi_M = (N\mathbf{g}^2\beta^2/3kT)\frac{[\sum_i S_i(S_i + 1)(2S_i + 1)\exp(-E_i/kT)]}{[\sum_i (2S_i + 1)\exp(-E_i/kT)]} \quad (3)$$

from the temperature-dependent Van Vleck equation, and an additional Curie term to fit small fractions, $P$, of the manganese dimers as a monomeric Mn(III)($S = 2$) impurity, shown in eq 4. The values $E_i$ are the energies of the different spin states of

$$\chi_M' = (1 - P)\chi_M + 2P(N\mathbf{g}^2\beta^2/3kT)[(2)(2 + 1)] \quad (4)$$

the dinuclear center derived using eq 5, where $S_i$ is the total spin of the dimer and $S_1 = S_2 = 3/2$. In these fits of the data,

$$E_i = -J[S_i(S_i + 1) - S_1(S_1 + 1) - S_2(S_2 + 1)] \quad (5)$$

the value of $J$ and the percentage of $S = 2$ (Mn(III)) impurity, $P$, were allowed to vary. The value of **g** either was allowed to vary or was fixed at 2.00. Since the Mn(IV) ions have a quartet ground state and thus no in-state spin−orbit coupling, they are not expected to have **g** values which deviate significantly from 2.00. Allowing **g** to vary did not substantially improve the fits or change the trends in $J$ values between the different complexes, so we report the values obtained from the fits with **g** fixed at 2.00. The fits shown by the solid lines in Figure 4 were obtained in this manner.

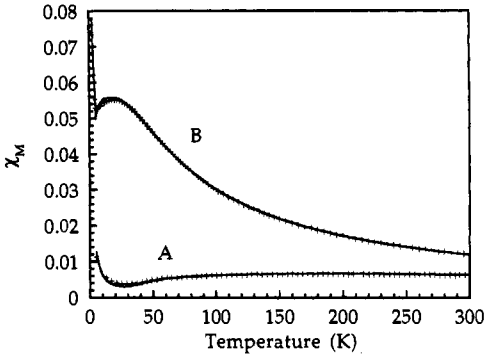


**Figure 5.** Temperature dependence of $\chi_M$ for (A) **1**H($CF_3SO_3$) and (B) **1**$H_2(CF_3SO_3)_2$. Data are represented by plus signs. The solid line is the best fit with **g** = 2.00 and $J$ and the percentage of $S = 2$ impurity allowed to vary, as described in the text. The $\chi_M$ vs $T$ data for **1**, not shown, agree with those reported by Gohdes and Armstrong.[16]

The value we obtain for the unprotonated **1** (A in Figure 4; $J = -92$ $cm^{-1}$) is approximately the same as that obtained by Gohdes and Armstrong[16] with **g** fixed at 2.00. As in their analysis, if **g** is allowed to vary, the value for $J$ drops by about 12 $cm^{-1}$, with a **g** value of about 1.8 providing the best fit. The fit of the data for **1** includes 0.4% of the manganese as a monomeric Mn(III) impurity. The analysis of **1**H($CF_3SO_3$) (B in Figure 4, A in Figure 5) gives a significantly decreased exchange interaction with $J = -48$ $cm^{-1}$ (1.0% $S = 2$ impurity) when **g** = 2.00. The second protonation, generating **1**$H_2(CF_3SO_3)_2$ (C in Figure 4, B in Figure 5), produces a weakly coupled dimer with $J = -6$ $cm^{-1}$ (2.3% $S = 2$ impurity). Variation of **g** in the fits of **1**H($CF_3SO_3$) and **1**$H_2(CF_3SO_3)_2$ causes little change in the calculated $J$ values and only small deviations from **g** = 2.00. The fits to the $\chi_M$ vs $T$ data for **1**H($CF_3SO_3$) and **1**$H_2(CF_3SO_3)_2$ using the same parameters as above are shown in Figure 5.

Variable temperature magnetic data were also obtained for the derivatives **2**−**5**, for which the reduction potentials and the p$K_a$'s of the protonated forms were shown to vary substantially with electron-donating and -withdrawing groups on the phenolate rings. The value of $J$ is found to be $-90 \pm 15$ $cm^{-1}$ for the complexes **1**−**5**, (**2**, $J = -75$ $cm^{-1}$; **3**, $J = -104$ $cm^{-1}$; **4**, $J = -104$ $cm^{-1}$; **5**, $J = -90$ $cm^{-1}$). There is no clear trend in these values which appears to correlate them with other physical properties of these $Mn_2O_2$ cores.[21] In order to confirm the dramatic decrease in the antiferromagnetic coupling of **1** upon protonation, the exchange interactions of the protonated derivatives of **5** were also determined. The complex **5** was shown to be the most dissimilar to **1** out of the series **1**−**5** in terms of the reduction potentials and the p$K_a$'s of the protonated forms. As shown by the values in Table 3, the sharp decrease in the exchange interaction occurs for the series **5**, **5**H($CF_3SO_3$), and **5**$H_2(CF_3SO_3)_2$ as well, again giving the extraordinarily weak exchange interaction in the doubly protonated species.

## Discussion

The bis($\mu$-oxo)manganese(IV) dimer [Mn(salpn)($\mu$-O)]$_2$, **1**, can be protonated on one [**1**H($CF_3SO_3$)] or both [**1**$H_2(CF_3SO_3)_2$] oxo bridges. *This series of complexes provides the first set of manganese complexes in which three protonation states of the*

*oxo bridges may be isolated without change in the oxidation state of the manganese.* The first protonation can be accomplished by a weak acid such as pyridinium. The protonation occurs on an oxo bridge as shown definitively by the 10 $cm^{-1}$ isotope shift in the frequency of the O−H stretch when the oxo bridges are labeled with $^{18}O$. The second oxo bridge may be protonated by a stronger acid (at −50 °C). The difference in p$K_a$ for the two protonations is 3−5 p$K_a$ units. Both protonations are reversible, and the unprotonated dimer can be regenerated by stoichiometric addition of base. While a number of unprotonated $Mn^{IV}_2(\mu\text{-}O)_2$ complexes have been characterized, this is the first isolation and characterization of a $Mn^{IV}_2(\mu\text{-}OH)_2$ complex. No such series exists for Fe, which shares a number of biological roles with manganese, either. While a number of $Fe^{III}_2(\mu\text{-}OH)_2$ complexes are known and the first $Fe^{III}_2(\mu\text{-}O,\mu\text{-}OH)$ complex has been recently reported,[28] no $Fe^{III}_2(\mu\text{-}O)_2$ complexes have been characterized. The series of complexes we report here allows the effects of successive protonations on such cores to be studied for the first time.

The lowest energy charge transfer (CT) transition, which is presumably a phenolate-to-manganese CT, shifts to lower energy by about 2200 $cm^{-1}$ with each protonation. This corresponds to a decrease in the electron density on the manganese, and the resulting decrease in the energy of the Mn d orbitals (the acceptor orbitals in the CT transition), with protonation of the oxo bridges. This is consistent with our earlier report showing a linear relationship between the reduction potential on the manganese and the p$K_a$ of the oxo bridge, indicating that the $Mn_2O_2$ core acts as a strongly coupled unit.[21]

The inflection points of the X-ray absorption edge spectra for the complexes **1**, **1**H($CF_3SO_3$), and **1**$H_2$($CF_3SO_3$)$_2$ all occur at about 6553 eV. This is significantly higher in energy than the edge energy for $Mn^{III}$(salpn)($CH_3OH$)$_2$. This confirms that the oxidation state of the manganese in these dimers does not change upon protonation. In addition, it shows that oxo bridge protonation does not significantly perturb the X-ray absorption edge of the oxo-bridged dimers. While protonation state changes on the oxo bridges might be considered as one way to produce shifts in the Mn edge energies in the OEC upon S-state advancement, the present data suggest that this is not likely. Thus, significant shifts observed in the edge energy upon changes in the OEC must result either from changes in the manganese oxidation state or from changes in the manganese coordination environment that are much more substantial than protonation of the oxo bridges.

Analysis of the EXAFS data for **1**, **1**H($CF_3SO_3$), and **1**$H_2$($CF_3SO_3$)$_2$ shows that the Mn−Mn distance lengthens by 0.1 Å with each protonation, from 2.73 to 2.83 to 2.93 Å. Although the metal−oxo distance is resolvable in the EXAFS spectra of a number of iron complexes containing oxo bridges,[27,28] the Mn−phenolate distances in the complexes reported here are sufficiently similar in length to the Mn−oxo and Mn−hydroxo distances to prevent their resolution in fits of the first shell of the EXAFS data. Thus, these data do not allow us to determine the specific distortions which occur in the $Mn_2O_2$ core upon protonation and lengthening of the Mn−Mn vector. The distortion in the least symmetric, singly protonated complex, **1**H($CF_3SO_3$), is likely to be similar to that recently determined for a $Fe_2(\mu\text{-}O,\mu\text{-}OH)$ complex,[28] in which the Fe−oxo distances (1.82 Å) are 0.17 Å shorter than the Fe−hydroxo distances (1.99 Å) and the Fe−oxo−Fe angle is substantially greater (106°) than the Fe−hydroxo−Fe angle (94°).

The temperature dependence of the magnetic susceptibility of **1** is identical to that reported previously by Gohdes and Armstrong.[16] The strong antiferromagnetic interaction observed in **1** ($J = -92$ $cm^{-1}$) decreases dramatically upon successive protonations [**1**H($CF_3SO_3$) ($J = -48$ $cm^{-1}$) and **1**$H_2$($CF_3SO_3$)$_2$ ($J = -6$ $cm^{-1}$)]. The weak antiferromagnetic interaction observed in **1**$H_2$($CF_3SO_3$)$_2$ is unprecedented for Mn(IV) dimers. In order to determine whether such a substantial decrease in the antiferromagnetic coupling is a general characteristic of protonating this type of complex, the series of complexes **5**, **5**H($CF_3SO_3$), and **5**$H_2$($CF_3SO_3$)$_2$ were prepared. Due to the addition of the strongly electron-withdrawing $NO_2$ groups to the phenolate rings of salpn, the reduction potential of **5** is over 500 mV higher than that of **1**, and the p$K_a$ of **5**H($CF_3SO_3$) is 6.6 units lower than that of **1**H($CF_3SO_3$). However, the magnetic behavior of **5** and **1** upon successive protonations is remarkably similar, with a dramatic decrease in the coupling observed for both series (Table 3). The $J$ values for the unprotonated complexes with various electron-donating and -withdrawing groups on salpn, **1**−**5**, are very similar ($J = -90 \pm 15$ $cm^{-1}$). No clear trend in the $J$ values is observed which may be correlated to the trends in reduction potential and p$K_a$ shown in Table 1.

The observed decrease in the exchange coupling between Mn(IV) ions resulting from protonation of the oxo bridges has important implications in interpreting the changes in magnetic behavior of the OEC upon S-state advancement and changes in configuration. While the changes in exchange coupling of the dimer are easily observed, competing exchange pathways in a tetranuclear cluster cause significant complications in determining the individual coupling constants. Kirk, et. al.[29] showed that exchange pathways in tetranuclear clusters that differ by an order of magnitude may even cause an apparent change in sign of the interdimer exchange interaction. In a "dimer of dimers" $[Mn^{III}Mn^{IV}]_2$ complex, in which two strongly coupled mixed valent dimers are linked by longer (~3.9 Å) alkoxide bridges, there is an apparent *ferromagnetic* coupling between two $S' = 1/2$ dimers, even though each individual exchange pathway in the cluster was shown to be *antiferromagnetic*.[29] Similarly, modifications of exchange pathways in the OEC caused by protonation could cause changes in the manifold of spin states of the cluster which would not be straightforward to interpret in terms of which individual exchange interactions are perturbed. Hagen et al.[30] have reported that the single protonation of an adamantane-type $[Mn_4O_6]^{4+}$ structure causes a change from *ferromagnetic* coupling in the unprotonated complex to *antiferromagnetic* coupling in the protonated complex. This seems contrary to the results reported here, although each pair of Mn(IV) ions in that structure have single oxo bridges. In addition, the complications noted by Kirk et al. may apply to the adamantane case as well.

Recently, Liang et al. reported that EXAFS spectra of the OEC in the $S_2$ configuration that is characterized by a $\mathbf{g} = 4$ EPR signal is best fit with two different Mn−Mn distances of 2.72 and 2.85 Å, although the "multiline EPR" configuration of $S_2$ requires only the shorter distance.[31] They suggest that this difference is due to binding of $Cl^-$ to one manganese in the multiline configuration, where a different ligand, such as water, is bound in the "$\mathbf{g} = 4$" configuration in a dimer of dimers model for the OEC. The data for **1**, **1**H($CF_3SO_3$), and **1**$H_2$($CF_3SO_3$)$_2$, however, suggest that such a change in bond lengths could also occur upon the protonation of one oxo bridge in one of the dimers. The reported change in Mn−Mn distance, as

(29) Kirk, M. L.; Chan, M. K.; Armstrong, W. H.; Solomon, E. I. *J. Am. Chem. Soc.* **1992**, *114*, 10432−10440.

(30) Hagan, K. S.; Westmoreland, T. D.; Scott, M. J.; Armstrong, W. H. *J. Am. Chem. Soc.* **1989**, *111*, 1907−1909.

(31) Liang, W.; Latimer, M. J.; Dau, H.; Roelofs, T. A.; Yachandra, V. K.; Sauer, K.; Klein, M. P. *Biochemistry* **1994**, *33*, 4923−4932.

well as the change in the ground spin state [*vide supra*], between the two $S_2$ configurations may be more likely to be caused by protonation of an oxo bridge than by the displacement of one terminal ligand.

In conclusion, we have prepared the first series of complexes in which the bridges of a $[Mn(IV)(\mu\text{-}O)]_2$ core may be successively protonated by one or two protons without a change in oxidation state, and all three protonation states have been isolated. Each protonation causes an increase in the Mn−Mn distance of 0.1 Å and a dramatic decrease in the antiferromagnetic coupling between Mn(IV) ions. The structural and magnetic effects of oxo bridge protonation are likely to be important in understanding the observed changes in the OEC upon *S*-state advancement and changes in the configurations of $S_1$ and $S_2$. The doubly protonated species is unstable in solution at room temperature, consistent with the previous observation by Boucher and Coe[32] that addition of perchloric acid to a similar $[Mn^{IV}(\mu\text{-}O)]_2$ complex resulted in decomposition to a Mn(III) species. Our isolation of $\mathbf{1}H_2(CF_3SO_3)_2$ allows us to probe this important proton-triggered manganese reduction reaction in more detail, and this will be discussed in a future paper.[33]

**Acknowledgment.** The authors are grateful to Andrew Gelasco and Neil Law (The University of Michigan) for helpful suggestions and other contributions and Professor Jack Norton, Jim Carroll, and Kurt Kramarz (Colorado State University) for useful discussions. This work was supported by NIH Grant No. GM39406 (V.L.P.), NIH postdoctoral fellowship (M.J.B.) Grant No. GM15102, and NIH Grant No. GM45205 (J.E.P.-H.). SSRL (Stanford Synchrotron Radiation Laboratory) and NSLS (National Synchrotron Light Source) are funded by the Department of Energy, Office of Basic Energy Sciences. The Biotechnology Program at SSRL is supported by the National Institutes of Health, Biomedical Research Training Program, National Center for Research Resources.

(32) Boucher, L. J.; Coe, C. G. *Inorg. Chem.* **1975**, *14*, 1289−1295.

(33) Baldwin, M. J.; Law, N. A.; Pecoraro, V. L. Manuscript in preparartion.

(34) Kristjánsdóttir, S. S.; Norton, J. R. In *Transition Metal Hydrides*; Dedieu, A., Ed.; VCH Publishers: New York, 1992; pp 309−359.